Evidence for distal transport of reworked Andean tephra: extending the cryptotephra framework from the Austral Volcanic Zone

A.J. Monteath[1*], P.D.M. Hughes[1], S. Wastegård[2]

[1]Geography and Environmental Science, University of Southampton, Southampton SO17 1BJ, UK
[2]Department of Physical Geography, Stockholm University, Stockholm SE-10691, Sweden

Abstract

Cryptotephra deposits (non-visible volcanic ash beds) may extend thousands of kilometres and provide valuable chronological isochrons. Here, we present a Lateglacial-early Holocene (c. 16,500 cal yr BP-6,000 cal yr BP) tephrostratigraphy from Hooker's Point, East Falkland, South Atlantic. This period spans the last glacial termination across the southern mid-latitudes, a time period during which the palaeoenvironmental record is poorly resolved in southern South America and the South Atlantic. The development of a regional tephrostratigraphy will provide chronological constraint for palaeoenvironmental records from this period. Two cryptotephra deposits from Hooker's Point are linked with Mt. Burney, including the early-Holocene MB_1 tephra, while a third is likely to be derived from the R_1 eruption of Reclus volcano. The high shard abundance of these cryptotephra deposits suggests they extend further into the Southern Ocean, and may act as regional stratigraphic markers during the Lateglacial. Further peaks in shard abundance are composed of detrital glass (tephra not derived from primary air fall events), with mixed shard morphologies and geochemically heterogeneous glass populations. This detrital glass is likely to have been repeatedly reworked by wind action in the Patagonian Steppe before final deposition in the Falkland Islands. The high abundance of detrital glass in the Hooker's Point sequence suggests long distance transport of reworked tephra is common in this region, and highlights the need to carefully analyse cryptotephra deposits in order to avoid incorrectly describing reworked tephra as new isochrons. A temporal pattern of shard abundance is apparent in the Hooker's Point sequence with a reduction /absence of shards between 14,300-10,500 cal yr BP.

KEYWORDS: Cryptotephra, Falkland Islands, Austral Volcanic Zone, Tephrochronology, Reworking

1. Introduction

Cryptotephra deposits (non-visible volcanic ash beds) provide valuable chronological isochrons, and insights into tephra transport and dispersal (Jensen *et al.,* 2014; Bronk Ramsey *et al.,* 2015; Plunkett and Pilcher, 2018). However, few cryptotephras deposits have been described from southern South America and the South Atlantic; a region affected by strong atmospheric circulation patterns and frequent explosive volcanism. Contemporary observations suggest tephra from this region may be deposited across wide areas. For example, ash from the 2011 eruption of the Puyehue-Cordón Caulle volcanic complex in Chile (Volcanic Explosivity Index; VEI 5) reached the Western Antarctic Ice Sheet

(Koffman *et al.,* 2017), and caused air traffic disruption in Australia and New Zealand (Klüser *et al.,* 2012; Alloway *et al.*, 2015). It is therefore likely that the palaeoenvironmental record holds further examples of distal cryptotephra deposits that may be used to synchronise climate archives and refine volcanic hazard assessments.

Here, we describe the Lateglacial and early Holocene (c. 16,500-6,000 cal yr BP) tephrostratigraphy from Hooker's Point (HP) (51°42'S, 57°47'W), an exposed peat cliff on East Falkland near Port Stanley (Fig. 1). This period spans the last glacial termination across the southern mid-latitudes, which was punctuated by abrupt climate events and changes in latitudinal positon and strength of the Southern Westerly Wind belt (SWW) (Vanneste *et al.,* 2015; Mayr *et al*., 2013; Moreno *et al.,* 2012). The palaeoenvironmental record from southern South America and the South Atlantic is poorly resolved during this period (Kilian and Lamy, 2013), with some sites recording uninterrupted warming (Haberle and Bennett, 2004), while others show dynamic osilations in temperature or precipitation (García *et al*., 2012; Mansilla *et al.,* 2018). This inconsistent, often contradictory, climate-record may reflect; i) differing proxy sensitivities, ii) real spatial-temporal climate variability or iii) chronological uncertainty, and the establishment of a regional tephrochronological framework will provide chronological constraint in addressing palaeoenvironmental questions.

The Falkland Islands (Islas Malvinas) are well placed to extend the tephrostratigraphy of southern South America as they lie beneath the central jet of the SWW (50-55°S), and downwind of the Andean Southern Volcanic Zone (SVZ; 33-46 °S) and the Austral Andean Volcanic Zone (AVZ; 49-55°S). Since the last glacial period 74 volcanic centres in these zones are known to have been active (Fontijn *et al.,* 2014, 2016), and cryptotephra deposits in Isla de los Estados (Unkel *et al.*, 2008), the Falkland Islands (Hall *et al.,* 2001), South Georgia (Oppedal *et al.,* 2018) and the Antarctic ice cores (Kurbatov *et al.,* 2006; Narcisi *et al.,* 2012) have been linked with Andean volcanoes. The Falkland Islands are therefore ideally placed to study palaeo-ash clouds extending from the Southern Andes during the Lateglacial-Holocene transition.

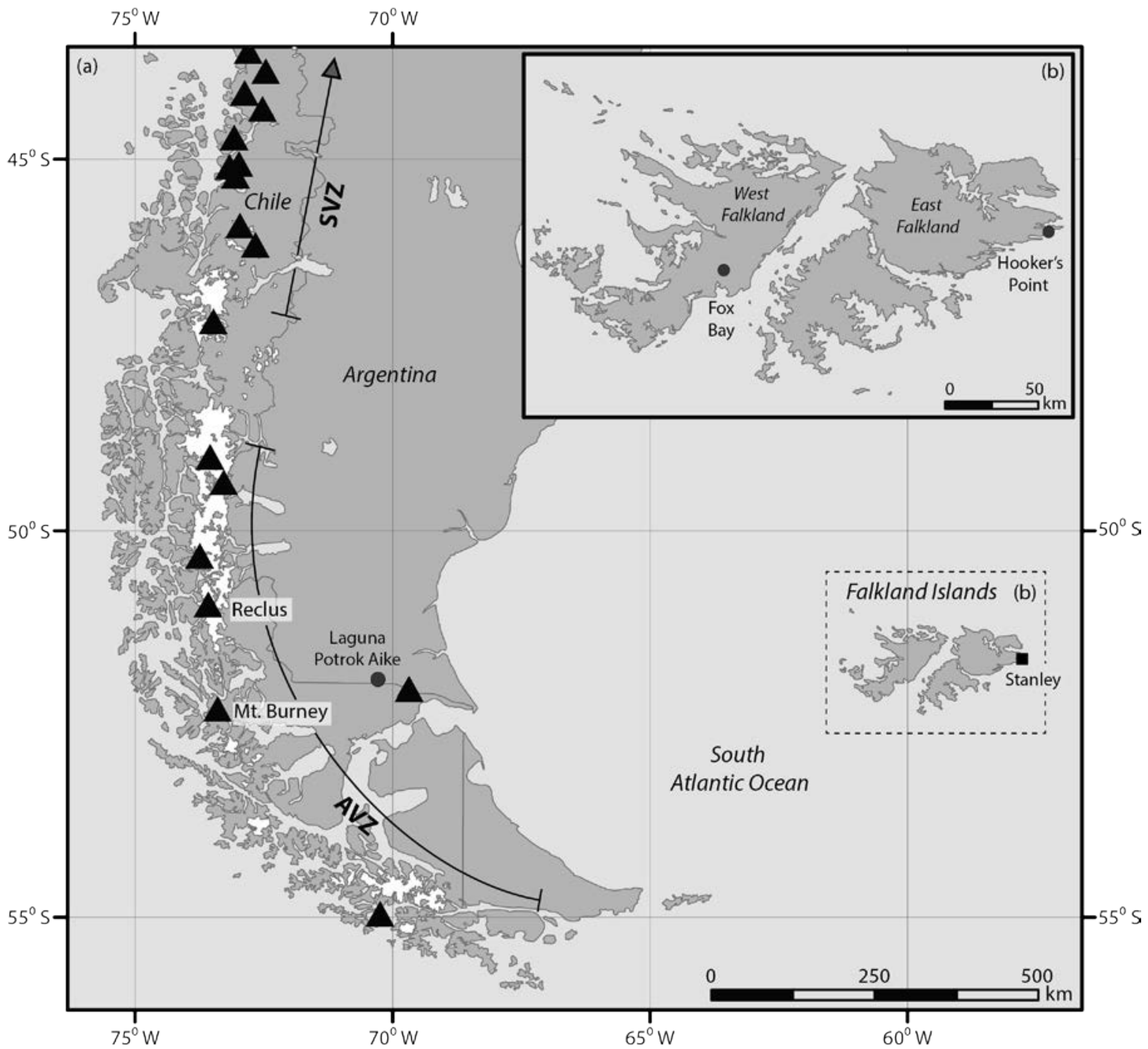

Figure 1: The position of sites and volcanoes described in the text. South American volcanoes known to have been active during the Holocene and Late-glacial are shown as black triangles (Smithsonian Global Volcanism programme, 2018). The extents of the Andean Southern Volcanic Zone (SVZ) and the Austral Andean Volcanic Zone (AVZ) are based those defined by Naranjo and Stern, (2004).

2. Materials and methods

2.1 The Hooker's Point section

The Hooker's Point peat sequence (51°42'S, 57°47'W), is situated in East Falkland, 3.5 km east of Port Stanley. The exposed section lies adjacent to Hooker' Point, immediately behind a small beach, and extends from around three metres a.s.l. to the cliff top at around eight metres a.s.l. The peat profile was sampled using a series of 50 cm and 25 cm monolith tins which were pushed into overlapping, cleaned, cliff sections. Samples beneath the present beach level were obtained using a hand gouge to a depth of two metres.

2.2 Tephrostratigraphy

Cryptotephra deposits were identified from continuous 5 cm samples, concentrated using ashing (Pilcher and Hall, 1992), emersion in 10 % Hydrochloric acid (HCl), and sieving (80 µm and 15 µm). Heavy liquid flotation at 2.0 g/cm^{-3} and 2.55 g/cm^{-3}, was used to extract glass shards from the remaining host material (Turney *et al.,* 1998), and residues were mounted in Canada Balsam and counted under a high power microscope. Shard abundance was quantified against the dried sample weight (shards/gram), as sample densities varied with organic content. Where peaks in shard abundance were identified, further 1 cm samples were processed and quantified in the same manner to refine the stratigraphic position of the cryptotephra deposit. The morphological characteristics of 100 glass shards from each cryptotephra deposit were recorded (colour, morphology and long axis length) and measured using an eyepiece graticule mounted in the high power microscope.

Glass shards from peak cryptotephra concentrations were extracted for electron probe microanalysis (EPMA) using heavy liquid flotation (Turney *et al.,* 1998) with minor modifications to the method; i) 10 % HCl was not applied as no carbonates were present in the samples, and ii) cleaning floats at 2.0 g/cm^{3} were retained and subjected to additional centrifuge cycles. Between these cycles samples were carefully stirred to separate glass shards from the organic material. Additional material from cryptotephra deposit HP_32 was subjected to acid digestion (Dugmore *et al.,* 1992) to increase the number of shards available for EPMA. Glass shards extracted for geochemical analysis were mounted in an epoxy resin stub and polished to expose internal glass surfaces before being carbon coated for EPMA.

The geochemical composition of glass shards were analysed following established protocols (Jensen *et al.,* 2008) at the University of Alberta, using wavelength dispersive spectrometry (WDS) on a JEOL 8900 superprobe and a Cameca SX-100 electron microprobe. Ten major-minor elements (Si, Ti, Al, Fe, Mn, Mg, Ca, Na, K, Cl) were measured using a 5 µm beam, with 15 keV accelerating voltage, and 6 nA beam current to minimise Na and K migration during analyses. Two secondary standards, of known composition, were run concurrently during EPMA to assess analytical accuracy and precision: i) ID3506, Lipari rhyolitic obsidian, and ii) Old Crow tephra (Kuehn *et al.,* 2011). Results were normalized to 100 % and are presented as weight percent oxides (wt %) in bi-plot diagrams (Fig. 3). Raw major-minor element glass compositions and associated standard measurements are reported in supplementary information Appendix B (Tables B1, B2).

2.3 Chronology

A Bayesian age-depth model (Fig 2.) was developed from eight radiocarbon dates (Table 1) using OxCal 4.2.3 (Bronk Ramsey, 2017), and the SHCal13 calibration curve (Hogg *et al.,* 2013). A *P_Sequence* depositional model was run with outlier detection (Bronk Ramsey, 2009a, 2009b), and a variable *k* factor (depositional events per unit length: cm^{-1}) (Bronk Ramsey and Lee, 2013). One radiocarbon date (Beta-241336) suggested a slight age reversal; however, it did not reduce the overall model agreement to <60 %, and so was retained in the final age-depth model (Bronk Ramsey, 2009a). Calibrated dates and age ranges are reported at two sigma (95.4 %) confidence throughout this study.

Table 1: Radiocarbon dates from the Hooker's Point sediment sequence with calibrated two sigma age ranges. Ages were calibrated using OxCal 4.2.3 (Bronk Ramsey, 2017), and the SHCal13 calibration curve (Hogg et al., 2013).

Laboratory ID Code	Material	Depth (cm)	Radiocarbon age (^{14}C yr BP)	13δC (‰)	Calibrated age range (95.4 %) (cal yr BP)
Beta-193400	Bulk (peat)	0-2	5700±40	-27.0	6628-6405

Beta-241334	Plant Macro	42-43	7390±40	-29.7	8341-8055
Beta-193401	Bulk (peat)	76	9250±80	-26.7	10650-10241
Beta-241335	Plant Macro	90-91	10030±40	-25.0	11749-11330
Beta-241336	Wood	94-95	9940±40	-27.0	11602-11242
Beta-193402	Bulk (peat)	100	10370±60	-27.3	12517-12000
Beta-241338	Plant Macro	154-155	13320±50	-27.1	16217-15822
Beta-193403	Bulk (peat)	168	13630±140	-27.7	16923-16055

3. Results and Discussion

High numbers of glass shards were found throughout large sections of the Hooker's Point sediment sequence, with increased tephra abundance between 65-75 cm and 130-174 cm (Fig. 2, A1). Samples from eight peaks in shard concentration were analysed by EPMA, all of which are composed of high SiO_2 rhyolitic glass (Table 2a). Three cryptotephra deposits are linked with volcanic centres in the Andean Austral volcanic zone (AVZ) based on the major-minor element composition of volcanic glass and modelled age ranges (Section 3.1). Analyses from further cryptotephra deposits are geochemically heterogeneous with low analytical totals (not reflected in secondary standards), low Na_2O and high SiO_2 (Table 2b, Fig. 3). These characteristics are found in heavily weathered detrital glasses (glass shards not derived from primary air fall events) which are susceptible to Na loss during analysis (Jensen *et al.,* 2016), and suggest a large amount of reworked glass is present in the Hooker's Point record.

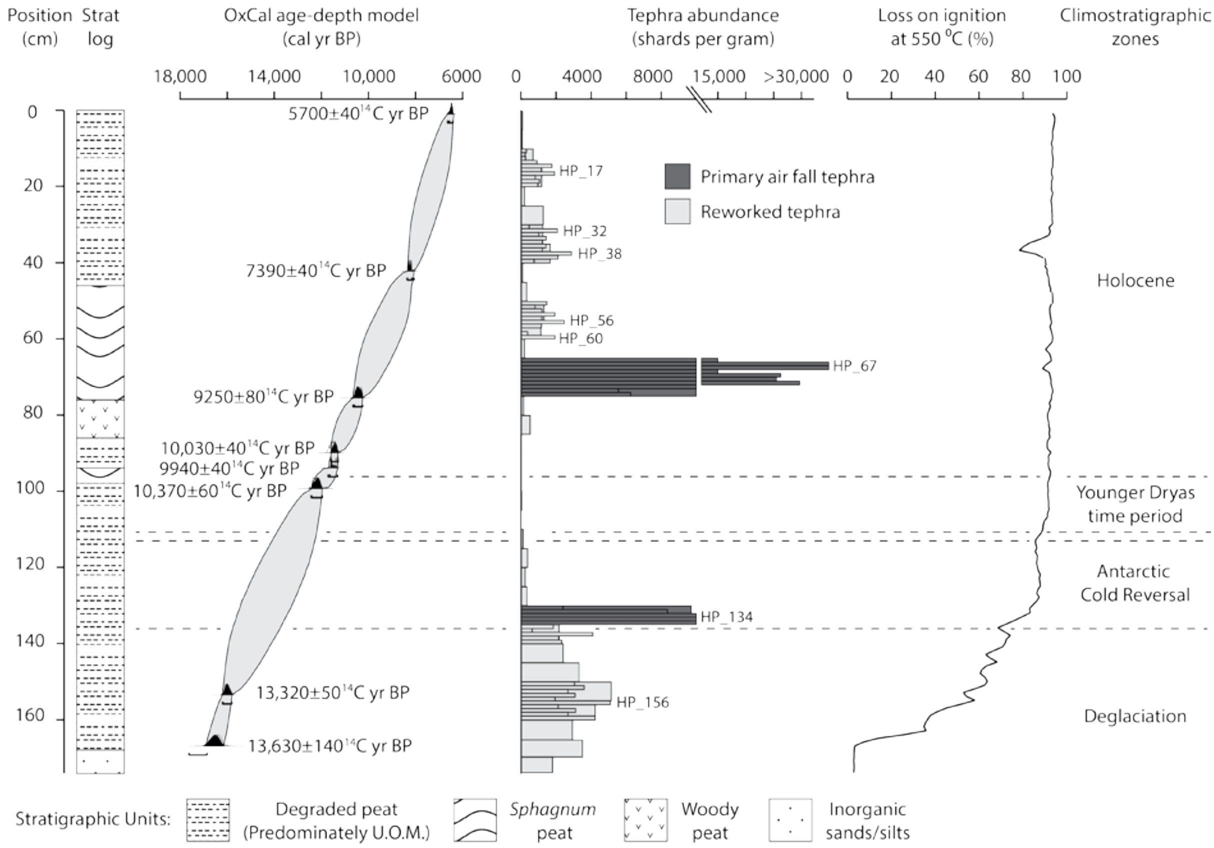

Figure 2: Summary lithostratigraphy, radiocarbon dates, OxCal age-depth model, tephra abundance, loss on ignition (LOI) and broad climatic zones from Hooker's Point, Falkland Islands.

Table 2: Major-minor element composition (non-normalised) of primary (a) and reworked (b) cryptotephra deposits from Hooker's Point, shown as mean and one standard deviation (StDev) (n = number of analyses). (c) Bracketing analyses and recommended values (Kuehn et al., 2011) for secondary standards. (*) Recommended value.

(a)

Sample	n		SiO_2	TiO_2	Al_2O_3	FeO_T	MnO	MgO	CaO	Na_2O	K_2O	Cl	Total
HP_14-17	10	Mean	75.58	0.17	12.81	1.02	0.03	0.26	1.18	4.15	1.96	0.20	97.32
Pop b.		StDev	*1.39*	*0.03*	*0.22*	*0.10*	*0.02*	*0.03*	*0.13*	*0.27*	*0.17*	*0.03*	*1.79*
HP_67	27	Mean	74.94	0.16	12.61	1.04	0.05	0.24	1.18	4.58	1.80	0.19	96.74
		StDev	*0.94*	*0.04*	*0.19*	*0.09*	*0.02*	*0.03*	*0.12*	*0.23*	*0.12*	*0.02*	*1.09*
HP_134	33	Mean	74.51	0.13	12.64	1.18	0.04	0.20	1.42	3.80	2.58	0.18	96.65
		StDev	*1.07*	*0.03*	*0.28*	*0.11*	*0.02*	*0.03*	*0.09*	*0.20*	*0.13*	*0.02*	*1.32*

(b)

Sample	n		SiO_2	TiO_2	Al_2O_3	FeO_T	MnO	MgO	CaO	Na_2O	K_2O	Cl	Total
HP_14-17	30	Mean	72.44	0.19	12.24	1.28	0.05	0.14	0.91	2.56	3.69	0.16	93.63
Detrital glass		StDev	*2.13*	*0.11*	*0.79*	*0.52*	*0.03*	*0.12*	*0.36*	*0.84*	*0.92*	*0.05*	*2.59*
HP_32	33	Mean	72.46	0.13	12.05	1.15	0.04	0.11	0.86	2.80	3.52	0.17	93.26
Detrital glass		StDev	*1.80*	*0.07*	*0.47*	*0.35*	*0.03*	*0.08*	*0.27*	*0.81*	*0.70*	*0.05*	*2.12*
HP_38	35	Mean	72.81	0.14	12.15	1.18	0.05	0.11	0.90	2.85	3.58	0.16	93.90
Detrital glass		StDev	*1.77*	*0.10*	*0.73*	*0.37*	*0.02*	*0.10*	*0.34*	*0.79*	*0.75*	*0.07*	*2.49*
HP_56	34	Mean	72.53	0.14	12.33	1.32	0.06	0.13	0.99	2.84	3.43	0.14	93.87
Detrital glass		StDev	*1.72*	*0.10*	*0.65*	*0.47*	*0.02*	*0.10*	*0.35*	*0.96*	*0.72*	*0.04*	*2.31*
HP_60	32	Mean	72.63	0.14	12.39	1.10	0.06	0.15	0.98	3.04	3.42	0.15	94.03
Detrital glass		StDev	*2.33*	*0.07*	*0.74*	*0.52*	*0.03*	*0.14*	*0.45*	*1.06*	*0.97*	*0.05*	*2.99*
HP_156	55	Mean	71.33	0.18	12.00	1.36	0.05	0.14	0.95	3.19	3.60	0.19	92.96
Detrital glass		StDev	*1.58*	*0.08*	*0.48*	*0.48*	*0.03*	*0.07*	*0.30*	*0.40*	*0.59*	*0.06*	*1.67*

(c)

Sample	n		SiO_2	TiO_2	Al_2O_3	FeO_T	MnO	MgO	CaO	Na_2O	K_2O	Cl	Total
Lipari	50	Mean	74.04	0.08	13.10	1.55	0.07	0.03	0.72	4.08	5.19	0.33	99.11
		StDev	*0.55*	*0.02*	*0.11*	*0.07*	*0.02*	*0.01*	*0.03*	*0.19*	*0.10*	*0.02*	*0.74*
Old Crow	41	Mean	72.1	0.3	12.62	1.61	0.06	0.29	1.40	3.78	3.63	0.27	95.99
		StDev	*0.83*	*0.04*	*0.14*	*0.07*	*0.02*	*0.03*	*0.05*	*0.19*	*0.15*	*0.02*	*1.11*
Lipari*	33	Mean	74.1	0.07	13.1	1.55	0.07	0.04	0.73	4.07	5.11	0.34	99.18
		StDev	*0.96*	*0.03*	*0.34*	*0.06*	*0.03*	*0.02*	*0.05*	*0.28*	*0.26*	*0.03*	
Old Crow*	18	Mean	72.1	0.3	12.5	1.62	0.05	0.28	1.43	3.66	3.56	0.27	95.77
		StDev	*1.7*	*0.05*	*0.3*	*0.12*	*0.02*	*0.02*	*0.05*	*0.38*	*0.28*	*0.05*	

Table 3: Shard morphology statistics for Hooker's Point cryptotephra deposits. Descriptions include: minimum (Min), maximum (Max) and mean ($\bar{x}$) long axis lengths (µm), as well as standard deviation (σ) and shard morphologies (SM). Descriptions are based on 100 measurements (n).

HP_17	HP_32	HP_38	HP_56	HP_60	HP_67	HP_134	HP_156
$\bar{x}$: 40	$\bar{x}$: 38	$\bar{x}$: 38	$\bar{x}$: 40	$\bar{x}$: 41	$\bar{x}$: 45	$\bar{x}$: 37	$\bar{x}$: 42
σ: 13	σ: 13	σ: 12	σ: 13	σ: 14	σ: 19	σ: 12	σ: 13
Max: 75	Max: 75	Max: 80	Max: 80	Max: 100	Max: 138	Max: 83	Max: 98
Min: 18	Min: 15	Min: 18	Min: 15	Min: 15	Min: 18	Min: 23	Min: 18
SM: mixed	SM: mixed	SM: mixed	SM: mixed	SM: mixed	SM: cuspate	SM: cuspate/platy	SM: mixed
n: 100	*n*: 100	*n*: 100	*n*: 100	*n*: 100	*n*: 100	*n*: 100	*n*: 100

3.1 Tephra correlations

Correlations between Hooker's Point cryptotephra deposits and Andean volcanoes are based on glass geochemical compositions, similarity coefficients (SC) (Borchardt *et al.,* 1972) and modelled age ranges; however, they should be considered as working correlations, to be continually tested by future studies. A future tephra framework for southern South American and the Southern Ocean should be based on a range of information including; glass geochemical compositions (major, minor and trace elements), petrology, chronology and stratigraphic context (Lowe *et al.,* 2017). This work is at an early stage in southern South America and there are few comparative datasets; however, recent studies are beginning to address this (Fontjin *et al.,* 2016; Del Carlo *et al.,* 2018; Mansilla *et al.,* 2018).

A consistent minor offset in SiO_2 and Al_2O_3 values is evident in tephras correlated between Hooker's Point and Laguna Potrok Aike (Fig 3). This offset is also apparent in the Lipari standard measurements (Fig. A4), which show no sign of Na loss (Tables B2, B4). The differences in SiO_2 and Al_2O_3 values are therefore likely to reflect differing instrumental conditions during EPMA. Future work could use side-by-side analysis of both samples to eliminate such analytical differences (Westgate *et al.,* 2013; Monteath *et al.,* 2017).

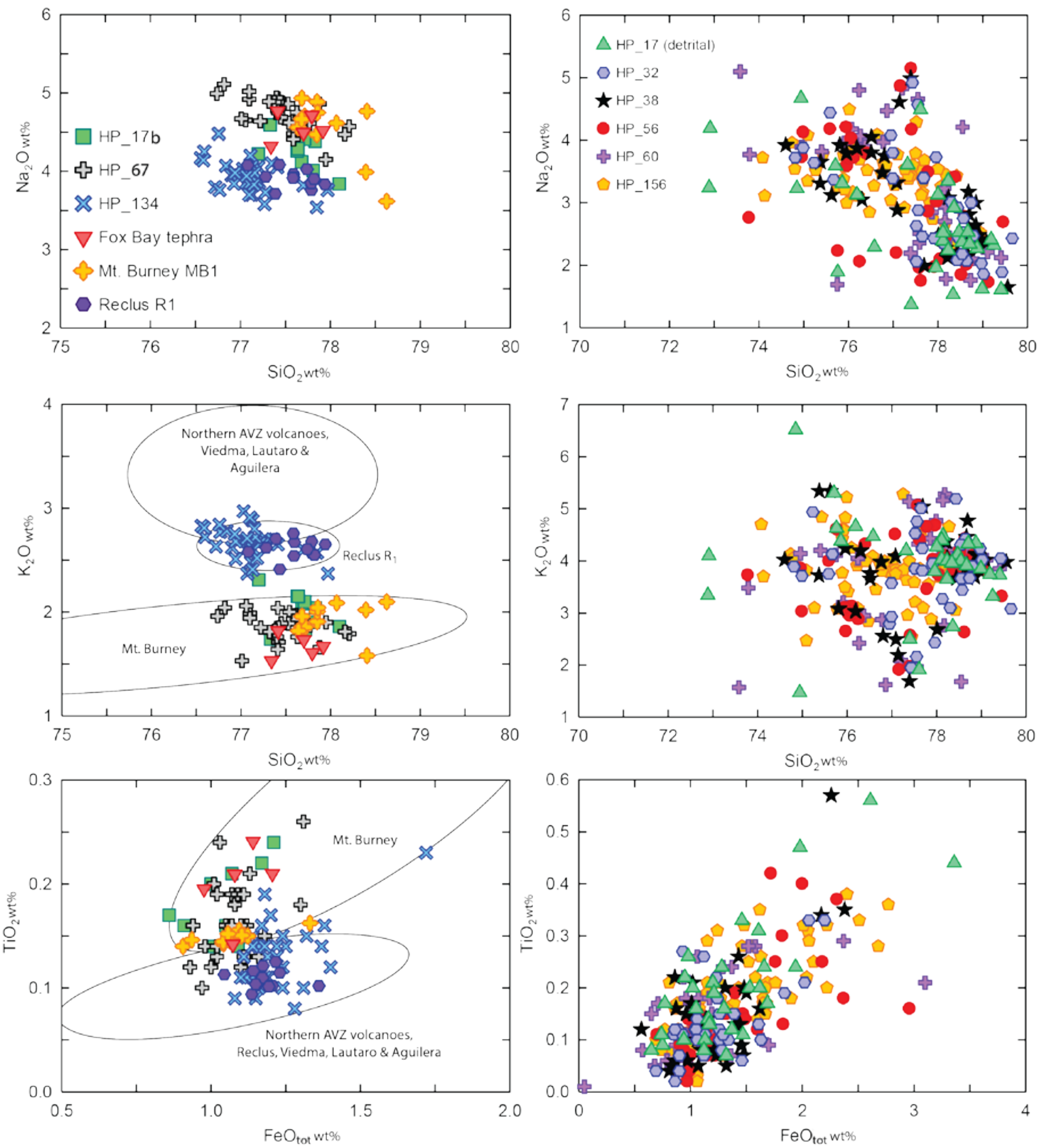

Figure 3: Bivariate plots of glass geochemical compositions (normalised major and minor element data) from Falkland Islands cryptotephra deposits (this study; Hall et al., 2001) and the Mb_1 and Reclus R_1 tephras from Laguna Potrok Aike (Wastegård et al., 2013). Geochemical envelopes are redrawn from Wastegård et al., (2013), and overlap previous studies of AVZ tephras (e.g. Kilian et al., 2003; Haberzettl et al., 2009; Stern, 2008). Colour version is available online.

3.1.1 Cryptotephra deposit HP_17 (14-17 cm)

HP_17 is composed of clear glass shards with mixed morphologies (Table 3, Fig. A2), and heterogeneous geochemical compositions (Fig. 3), suggesting that the majority of the cryptotephra deposit is formed of detrital glass. However, a sub population (n=10) (hereafter referred to as HP_17b) with low K_2O values (1.74-2.31 wt %) relative to other HP_17 analyses, plots consistently as a discrete group, and may be derived from a primary air fall event (Fig. 3). Analyses from this group closely overlap those from HP_67 except for marginally lower Na_2O values (Fig. 3).The two-sigma modelled age range of HP_17 is 7,680-6,610 cal yr BP. However, the age range of HP_17b cannot be precisely determined as consistent geochemical analyses only account for 25% (n=10) of the deposit, and the exact stratigraphic position of the cryptotephra may be obscured by detrital glass.

Glass geochemical compositions from HP_17b consistently plot as Mt. Burney 'type' and may be separated from other volcanic centres in SVZ and AVZ by high SiO_2 (77.2-78.1 wt%) and low K_2O values (1.74-2.31 wt%) (Kilian *et al.,* 2003; Haberzettl *et al.,* 2009; Stern, 2008; Wastegård *et al.,* 2013; Del Carlo *et al.,* 2018). No large eruptions of Mt. Burney are known from the modelled age range of HP_17, and HP_17b may represent a previously unknown eruption of this volcano. Alternatively, Kilian *et al.,* (2003) describe a Mt. Burney 'type' tephra bed stratigraphically between the MB_1 (9950-8850 cal yr BP; Stern *et al.,* 2008) and MB_2 (3820-4710 cal yrs BP; Del Carlo *et al*., 2018) tephras, also derived from Mt. Burney. The best age constraint for this eruption is a radiocarbon date (4420±40 ^{14}C yr BP) 17 cm above the tephra. Based on sediment accumulation rates, Kilian *et al.,* (2003) suggest an age of around 5691±11 cal yr BP for the described tephra bed. Given the dating uncertainties associated with both tephras, it's plausible that they may be derived from the same eruption; however, further understanding of the Mt. Burney eruptive history is needed to test both of these hypotheses.

3.1.2 Cryptotephra deposit HP_67 (67 cm)

HP_67 is a highly abundant cryptotephra deposit (>30,000 shards per gram), formed of clear, cuspate, glass shards (Table 3, Figs. A2, A5). Glass geochemical compositions occur in a narrow SiO_2 range (76.7-78.2 wt%), and have low K_2O values (1.53-2.06 wt%), relative to other cryptotephra deposits present in Hooker's Point, with the exception of HP_17b (Fig. 3). The two-sigma modelled age range of HP_67 is 10,490-9,190 cal yr BP.

Glass major-minor elements from HP_67 plot in high SiO_2 Mt. Burney envelopes (Fig. 3), and closely overlap the MB_1 tephra in Laguna Potrok Aike (Wastegård *et al.,* 2013) (SC: 0.96; Table B3) . The MB_1 tephra was deposited eastward from a large (VEI 5), early Holocene, eruption of Mt. Burney (Fontijn *et al.,* 2014), radiocarbon dated to 9950-8850 cal yr BP by Stern *et al.,* (2008). This age estimate overlaps with the modelled age range of HP_67, and HP_67 may be correlated with the MB_1 tephra. This correlation extends the known distribution of this ash deposit >1,000 km east from Mt. Burney.

3.1.3 Cryptotephra deposit HP_134 (132-135 cm)

HP_134 forms an abundant (>12,000 shards per gram) cryptotephra deposit composed of clear, cuspate, platy, shards (Table 3, Figs. A2, A5). Glass shard geochemical compositions fall in a tight high SiO_2 range (76.5-78 wt%), with intermediate K_2O values (2.37-2.97 wt%) relative to other Hooker's Point cryptotephra deposits. The two-sigma modelled age range of the cryptotephra deposit is 15,640-13,550 cal yr BP.

The geochemical composition of glass analyses from HP_134 consistently plot in major-minor element envelopes for Reclus volcano (Fig. 3), and closely overlap the Reclus R_1 tephra in Laguna Potrok Aike (Wastegård *et al.,* 2013) (SC: 0.95; Table B3). Published age ranges for the Reclus R_1 tephra (15,510-14,350 cal yr BP; McCulloch *et al.,* 2005; 15,260-14,370 cal yr BP; Stern *et al.,* 2008) overlap the modelled age range of HP_134, and it is likely that HP_134 may be correlated with Reclus R_1. This tephra was deposited to the southeast of Reclus Volcano, towards the Falkland Islands, and is derived from one of the largest eruptions known from the AVZ (VEI 6) (Stern *et al.,* 2011; Fontijn *et al.,* 2014).

Identification of the Reclus R_1 tephra in East Falkland extends the known distribution of this ash deposit >1,100 km from Reclus volcano.

3.1.4 Fox Bay cryptotephra deposit 60-65 cm

Comparison between published EPMA data from Fox Bay, West Falkland (Hall *et al.,* 2001), and analyses from Laguna Potrok Aike (Wastegård *et al.,* 2013) and Hooker's Point (Fig. 3), show a strong geochemical overlap between an uncorrelated cryptotephra deposit in Fox Bay at 60-65 cm, and Mt. Burney 'type' analyses. The Fox Bay cryptotephra deposit is undated and so cannot be linked with an eruption event; however, the analyses suggest Mt. Burney 'type' cryptotephra deposits may be present across the Falkland Islands.

3.2 Detrital glass abundance

The majority of cryptotephra deposits analysed from Hooker's Point are composed of detrital glass (glass shards not derived from primary air fall events) with heterogeneous glass geochemistries (Fig 3). No visible tephra beds have been reported from the Falkland Islands (Hall *et al.,* 2001) that could act as sources of reworked glass, and it is likely that detrital glass present in Hooker's Point is reworked from deposits in southern South America. Prevailing westerly winds and outwash plains mean tephra from volcanic eruptions in the SVZ and the AVZ is widely deposited over the Patagonian steppe. In this semi-arid, sparsely vegetated, environment tephra may be repeatedly reworked by wind action where it forms a large component of regional dust emissions (Gaiero *et al*., 2007). Unconsolidated tephra, can be suspended by relatively low winds speeds (6-9 km/h) (Fowler and Lopushinsky, 1986), and once remobilised tephra from southern South America may be transported and deposited over large distances (including the Falkland Islands). For example, in the aftermath of the 1991 eruption of Volcán Hudson (VEI 5) plumes of remobilised ash extended >1000 km over Argentina and the western Atlantic Ocean (Wilson *et al.,* 2011). The discovery of abundant detrital glass throughout the Hooker's Point sediment sequence suggests that distal transport of reworked tephra is a common occurrence in this region, and that cryptotephra deposits must be carefully analysed in order to avoid incorrectly describing reworked material as new primary air fall events.

A temporal pattern of detrital glass abundance is apparent in the Hooker's Point sediment sequence, with an absence/reduction of tephra during the time periods associated with the Antarctic Cold Reversal (ACR; 14,700-13,000 cal yr BP; Pedro *et al*., 2011), Younger Dryas (YD; 12,900-11,700 cal yr BP; Walker *et al*., 2009), and early-Holocene (Fig 2). This pattern could reflect; i) changes in position and/or strength of the Southern Westerly Winds (SWW), with stronger winds delivering more detrital glass to the study site. However, while the dynamics of the SWW are poorly resolved during the Lateglacial palaeoenvironmental records from latitudes both North and South of the Falkland Islands suggest an increase in SWW velocities during the ACR (Moreno *et al.,* 2012; Vanneste *et al.,* 2015), which is not reflected in the detrital glass record from Hooker's Point. ii) Alternatively, tephra abundance could indicate changes in eruption frequency from the SVZ and AVZ. Several studies have discussed a link between deglaciation and increasing volcanism (Watt *et al.,* 2013; Fontijn *et al.,* 2016; Weller *et al.,* 2018); however, the low Na_2O and high SiO_2 values in detrital tephra from Hooker's Point suggest that the glass has been subjected to extensive weathering prior to deposition. This weathering indicates a lag between the eruptive event and final burial of the glass at Hooker's Point. Therefore the tephra delivery pattern may not reflect the eruption sequence as primary air fall events are rapidly transported and deposited. Finally, the temporal pattern may be derived from iii) site specific taphonomic processes and changes in the efficiency of tephra entrapment. Each of these hypotheses could explain the temporal pattern of tephra abundance in Hooker's Point, and further investigation of the sedimentary (e.g. grain size analysis) and dust (e.g. rare earth elements) records from Hooker's Point are needed to disentangle potential taphonomic and climatic influences on the detrital glass signal.

The abundant detrital glass present in Hooker's Point is likely to obscure a more comprehensive tephrostratigraphy. Numerous large explosive eruptions are known to have taken place in the SVZ and AVZ since deglaciation, which were deposited eastward across large areas (Fontijn *et al.,* 2014, 2016). Tephra from these eruptions is likely to be present in Hooker's Point, but are obscured by the influx of detrital tephra. Morphological descriptions of the Hooker's Point cryptotephra deposits show that although there is little variance in shard size (Fig A2) primary air fall events (HP_67 and HP_134) have more consistent shard morphologies than detrital glass deposits (Fig A3). Mclean *et al.,* (2018) used shard morphologies to differentiate between reworked tephra and primary air fall events in Japan, and this approach may allow detection of further cryptotephra deposits in the Falkland Islands.

4. Conclusions

Modern observations and palaeo records suggest that the study of cryptotephra deposits originating from Andean volcanoes is likely to provide valuable chronological isochrones across southern South America and the South Atlantic islands. The development of a Lateglacial tephrostratigraphy from this region will help answer questions of abrupt climate change during this period, which are poorly resolved at present.

Cryptotephra deposits in Hooker's Point are linked with the widespread MB_1 and R_1 tephras, which are likely to extend beyond the Falkland Islands, and may act as key regional markers. An additional Mt. Burney type cryptotephra, deposited during the mid-Holocene, may represent a minor eruption of Mt. Burney described by Kilian *et al.,* (2003), or a previously unknown eruption from the same source.

A high abundance of detrital glass is present throughout large sections of the Hooker's Point sediment sequence. This glass is likely to have been sourced from reworked deposits in southern South America, suggesting distal transport of reworked glass is common in this region, and care must be taken to avoid interpreting reworked deposits as new primary air fall events. A temporal pattern of detrital glass abundance is apparent in Hooker's Point, with a reduction in the concentration of shards throughout the ACR, YD period and early-Holocene. This pattern may reflect; i) variability in the strength and/or position of the SWW, ii) changes in eruption frequency, or iii) site-specific taphonomic processes; however, further work is needed to test these hypotheses.

Further primary cryptotephra deposits are likely to be obscured by detrital glass, and future studies of cryptotephra in the Falklands may benefit from a morphology-based approach to shard quantification.

Acknowledgements

We are grateful to Prof Robert Scaife, Prof Anthony Long and Prof Mike Bentley for access to the Hooker's Point peat sequence and radiocarbon dating. We would also like to thank Dr Lauren Davies and Prof Britta Jensen for their help with sample preparation and EPMA analysis at the University of Alberta. Fieldwork for this project was funded by the Shackleton trust, and was supported by the

Falkland Islands Bureau of Mineral Resources. Alex Blake assisted in sample collection from Hooker's Point and tephrochronology was supported by a World Universities Network Research Mobility Programme grant, awarded to Ali Monteath. We are also grateful to Peter Abbott and a second anonymous reviewer for their helpful comments on an earlier version of this manuscript.

References

Alloway, B.V., Pearce, N.J.G., Villarosa, G., Outes, V., Moreno, P.I., 2015. Multiple melt bodies fed the AD 2011 eruption of Puyehue-Cordón Caulle, Chile. Scientific reports 5, 17589.

Borchardt, G.A., Aruscavage, P.J., Millard, H.J., 1972. Correlation of the Bishop Ash, a Pleistocene marker bed, using instrumental neutron activation analysis. Journal of Sedimentary Research 42, 301–306.

Bronk Ramsey, C., 2009a. Bayesian analysis of radiocarbon dates. Radiocarbon 51, 337–360.

Bronk Ramsey, C., 2009b. Dealing with outliers and offsets in radiocarbon dating. Radiocarbon 51, 1023–1045.

Bronk Ramsey, C., Lee, S., 2013. Recent and planned developments of the program OxCal. Radiocarbon 55, 720–730.

Bronk Ramsey, C., Albert, P.G., Blockley, S.P., Hardiman, M., Housley, R.A., Lane, C.S., Lee, S., Matthews, I.P., Smith, V.C., Lowe, J.J., 2015. Improved age estimates for key Late Quaternary European tephra horizons in the RESET lattice. Quaternary Science Reviews 118, 18–32.

Bronk Ramsey, C., 2017. OxCal project, Version 4.3. Retrieved April 2018. https://c14.arch.ox.ac.uk/oxcal/OxCal.html.

Del Carlo, P., Di Roberto, A., D'Orazio, M., Petrelli, M., Angioletti, A., Zanchetta, G., Maggi, V., Daga, R., Nazzari, M. and Rocchi, S., 2018. Late Glacial-Holocene tephra from southern Patagonia and Tierra del Fuego (Argentina, Chile): A complete textural and geochemical fingerprinting for distal correlations in the Southern Hemisphere. Quaternary Science Reviews 195, 153–170.

Dugmore, A.J., Newton, A.J., Sugden, D.E., Larsen, G., 1992. Geochemical stability of fine-grained silicic Holocene tephra in Iceland and Scotland. Journal of Quaternary Science 7, 173–183.

Fontijn, K., Lachowycz, S.M., Rawson, H., Pyle, D.M., Mather, T.A., Naranjo, J.A., Moreno-Roa, H., 2014. Late Quaternary tephrostratigraphy of southern Chile and Argentina. Quaternary Science Reviews 89, 70–84.

Fontijn, K., Rawson, H., Van Daele, M., Moernaut, J., Abarzúa, A.M., Heirman, K., Bertrand, S., Pyle, D.M., Mather, T.A., De Batist, M., Naranjo, J.A., 2016. Synchronisation of sedimentary records using tephra: A postglacial tephrochronological model for the Chilean Lake District. Quaternary Science Reviews 137, 234–254.

Fowler, W.B., Lopushinsky, W., 1986. Wind-blown volcanic ash in forest and agricultural locations as related to meteorological conditions. Atmospheric Environment 20, 421–425.

Gaiero, D.M., Brunet, F., Probst, J.L., Depetris, P.J., 2007. A uniform isotopic and chemical signature of dust exported from Patagonia: Rock sources and occurrence in southern environments. Chemical Geology 238, 107-120.

García, J.L., Kaplan, M.R., Hall, B.L., Schaefer, J.M., Vega, R.M., Schwartz, R., Finkel, R., 2012. Glacier expansion in southern Patagonia throughout the Antarctic cold reversal. Geology 40, 859–862.

Global Volcanism Program: Smithsonian Institution. https://volcano.si.edu/ (15 March 2018)

Haberzettl, T., Anselmetti, F.S., Bowen, S.W., Fey, M., Mayr, C., Zolitschka, B., Ariztegui, D., Mauz, B., Ohlendorf, C., Kastner, S., Lücke, A., 2009. Late Pleistocene dust deposition in the Patagonian steppe-extending and refining the paleoenvironmental and tephrochronological record from Laguna Potrok Aike back to 55 ka. Quaternary Science Reviews 28, 2927–2939.

Hall, V.A., Wilson, P., Holmes, J., 2001. A preliminary tephra study of Holocene peats in the Falkland Islands. *Dossiers de l'Archäol-Logis* 1, 39–44.

Haberle, S.G. and Bennett, K.D., 2004. Postglacial formation and dynamics of North Patagonian rainforest in the Chonos Archipelago, Southern Chile. Quaternary Science Reviews 23, 2433–2452.

Hogg, A.G., Hua, Q., Blackwell, P.G., Niu, M., Buck, C.E., Guilderson, T.P., Heaton, T.J., Palmer, J.G., Reimer, P.J., Reimer, R.W., Turney, C.S., 2013. SHCal13 Southern Hemisphere calibration, 0–50,000 years cal BP. Radiocarbon 55, 1889–1903.

Jensen, B.J., Froese, D.G., Preece, S.J., Westgate, J.A., Stachel, T., 2008. An extensive middle to late Pleistocene tephrochronologic record from east-central Alaska. Quaternary Science Reviews 27, 411–427.

Jensen, B.J., Pyne-O'Donnell, S., Plunkett, G., Froese, D.G., Hughes, P.D., Sigl, M., McConnell, J.R., Amesbury, M.J., Blackwell, P.G., van den Bogaard, C., Buck, C.E., 2014. Transatlantic distribution of the Alaskan white river ash. Geology 42, 875–878.

Jensen, B.J., Evans, M.E., Froese, D.G., Kravchinsky, V.A., 2016. 150,000 years of loess accumulation in central Alaska. Quaternary Science Reviews 135, 1–23.

Kilian, R., Hohner, M., Biester, H., Wallrabe-Adams, H.J., Stern, C.R., 2003. Holocene peat and lake sediment tephra record from the southernmost Chilean Andes (53-55 S). Revista geologica de Chile, 30, 23–37.

Kilian, R., Lamy, F., 2013. A review of Glacial and Holocene paleoclimate records from southernmost Patagonia (49–55 ^{o}S). Quaternary Science Reviews 53, 1–23.

Klüser, L., Erbertseder, T., Meyer-Arnek, J., 2012. Observation of volcanic ash from Puyehue-Cordón Caulle with IASI. Atmospheric Measurement Techniques Discussions 5, 4249–4283.

Koffman, B.G., Dowd, E.G., Osterberg, E.C., Ferris, D.G., Hartman, L.H., Wheatley, S.D., Kurbatov, A.V., Wong, G.J., Markle, B.R., Dunbar, N.W., Kreutz, K.J., 2017. Rapid transport of ash and sulfate from the 2011 Puyehue-Cordón Caulle (Chile) eruption to West Antarctica. Journal of Geophysical Research: Atmospheres 122, 8908–8920.

Kuehn, S.C., Froese, D.G., Shane, P.A., Participants, I.I., 2011. The INTAV intercomparison of electron-beam microanalysis of glass by tephrochronology laboratories: results and recommendations. Quaternary International 246, 19–47.

Kurbatov, A.V., Zielinski, G.A., Dunbar, N.W., Mayewski, P.A., Meyerson, E.A., Sneed, S.B., Taylor, K.C., 2006. A 12,000 year record of explosive volcanism in the Siple Dome Ice Core, West Antarctica. Journal of Geophysical Research: Atmospheres, 111(D12).

Lowe, D.J., Pearce, N.J., Jorgensen, M.A., Kuehn, S.C., Tryon, C.A., Hayward, C.L., 2017. Correlating tephras and cryptotephras using glass compositional analyses and numerical and statistical methods: Review and evaluation. Quaternary Science Reviews 175, 1–44.

Mansilla, C.A., McCulloch, R.D., Morello, F., 2018. The vulnerability of the Nothofagus forest-steppe ecotone to climate change: Palaeoecological evidence from Tierra del Fuego (~53° S). Palaeogeography, Palaeoclimatology, Palaeoecology 508, 59–70.

Mayr, C., Lücke, A., Wagner, S., Wissel, H., Ohlendorf, C., Haberzettl, T., Oehlerich, M., Schäbitz, F., Wille, M., Zhu, J., Zolitschka, B., 2013. Intensified Southern Hemisphere Westerlies regulated atmospheric CO2 during the last deglaciation. Geology 41, 831–834.

McCulloch, R.D., Fogwill, C.J., Sugden, D.E., Bentley, M.J., Kubik, P.W., 2005. Chronology of the last glaciation in central Strait of Magellan and Bahía Inútil, southernmost South America. Geografiska Annaler: Series A, Physical Geography 87, 289–312.

McLean, D., Albert, P.G., Nakagawa, T., Suzuki, T., Staff, R.A., Yamada, K., Kitaba, I., Haraguchi, T., Kitagawa, J., Smith, V., 2018. Integrating the Holocene tephrostratigraphy for East Asia using a high-resolution cryptotephra study from Lake Suigetsu (SG14 core), central Japan. Quaternary Science Reviews 183, 36–58.

Monteath, A.J., van Hardenbroek, M., Davies, L.J., Froese, D.G., Langdon, P.G., Xu, X., Edwards, M.E., 2017. Chronology and glass chemistry of tephra and cryptotephra horizons from lake sediments in northern Alaska, USA. Quaternary Research 88, 169–178.

Moreno, P.I., Villa-Martínez, R., Cárdenas, M.L., Sagredo, E.A., 2012. Deglacial changes of the southern margin of the southern westerly winds revealed by terrestrial records from SW Patagonia (52 S). Quaternary Science Reviews 41, 1–21.

Naranjo, J.A., Stern, C.R., 2004. Holocene tephrochronology of the southernmost part (42 30'-45 S) of the Andean Southern Volcanic Zone. Revista geológica de Chile 31, 224–240.

Narcisi, B., Petit, J.R., Delmonte, B., Scarchilli, C., Stenni, B., 2012. A 16,000-yr tephra framework for the Antarctic ice sheet: a contribution from the new Talos Dome core. Quaternary Science Reviews 49, 52–63.

Oppedal, L.T., van der Bilt, W.G., Balascio, N.L., Bakke, J., 2018. Patagonian ash on sub-Antarctic South Georgia: expanding the tephrostratigraphy of southern South America into the Atlantic sector of the Southern Ocean. Journal of Quaternary Science. DOI: 10.1002/jqs.3035

Pedro, J.B., Van Ommen, T.D., Rasmussen, S.O., Morgan, V.I., Chappellaz, J., Moy, A.D., Masson-Delmotte, V., Delmotte, M., 2011. The last deglaciation: timing the bipolar seesaw. Climate of the Past 7, 671–683.

Pilcher, J.R., Hall, V.A., 1992. Towards a tephrochronology for the Holocene of the north of Ireland. Holocene 2, 255–259.

Plunkett, G., Pilcher, J.R., 2018. Defining the potential source region of volcanic ash in northwest Europe during the Mid-to Late Holocene. Earth-Science Reviews 179, 20–37.

Stern, C.R., 2008. Holocene tephrochronology record of large explosive eruptions in the southernmost Patagonian Andes. Bulletin of Volcanology 70, 435–454.

Stern, C.R., Moreno, P.I., Villa-Martinez, R., Sagredo, E.A., Prieto, A., Labarca, R., 2011. Evolution of ice-dammed proglacial lakes in Última Esperanza, Chile: implications from the late-glacial R1 eruption of Reclús volcano, Andean Austral Volcanic Zone. Andean Geology 38, 82–97.

Turney, C.S.M., 1998. Exatraction of rhyolitic component of Vedde microtephra from minerogenic lake sediments. Journal of Paleolimnology 19, 199–206.

Unkel, I., Björck, S., Wohlfarth, B., 2008. Deglacial environmental changes on Isla de los Estados (54.4°S), southeastern Tierra del Fuego. Quaternary Science Reviews 27, 1541–1554.

Vanneste, H., De Vleeschouwer, F., Martínez-Cortizas, A., Von Scheffer, C., Piotrowska, N., Coronato, A., Le Roux, G., 2015. Late-glacial elevated dust deposition linked to westerly wind shifts in southern South America. Scientific reports 5, 11670.

Walker, M., Johnsen, S., Rasmussen, S.O., Popp, T., Steffensen, J.P., Gibbard, P., Hoek, W., Lowe, J., Andrews, J., Björck, S. and Cwynar, L.C., 2009. Formal definition and dating of the GSSP (Global Stratotype Section and Point) for the base of the Holocene using the Greenland NGRIP ice core, and selected auxiliary records. Journal of Quaternary Science 24, 3–17.

Wastegård, S., Veres, D., Kliem, P., Hahn, A., Ohlendorf, C., Zolitschka, B., 2013. Towards a late Quaternary tephrochronological framework for the southernmost part of South America–the Laguna Potrok Aike tephra record. Quaternary Science Reviews 71, 81–90.

Watt, S.F., Pyle, D.M., Mather, T.A., 2013. The volcanic response to deglaciation: Evidence from glaciated arcs and a reassessment of global eruption records. Earth Science Reviews 122, 77–102.

Westgate, J.A., Pearce, N.J.G., Perkins, W.T., Preece, S.J., Chesner, C.A., Muhammad, R.F., 2013. Tephrochronology of the Toba tuffs: four primary glass populations define the 75 ka Youngest Toba Tuff, northern Sumatra, Indonesia. Journal of Quaternary Science 28, 772–776.

Weller, D.J., de Porras, M.E., Maldonado, A., Méndez, C., Stern, C.R., 2018. New age controls on the tephrochronology of the southernmost Andean Southern Volcanic Zone, Chile. Quaternary Research, doi.org/10.1017/qua.2018.81

Wilson, T.M., Cole, J.W., Stewart, C., Cronin, S.J., Johnston, D.M., 2011. Ash storms: impacts of wind-remobilised volcanic ash on rural communities and agriculture following the 1991 Hudson eruption, southern Patagonia, Chile. Bulletin of Volcanology 73, 223–239.